INTERACTION OF VORTICITY, RATE OF STRAIN, AND SCALAR GRADIENT IN STABLY STRATIFIED HOMOGENEOUS SHEARED TURBULENCE

Peter J. Diamessis and Keiko K. Nomura
Dept. of Applied Mechanics and Engineering Sciences
University of California, San Diego
La Jolla, CA 92093-0411, USA

ABSTRACT

The fully coupled, triadic interaction of vorticity ω, rate-of-strain S, and scalar (density) gradient $G \equiv \nabla\rho$ in stratified sheared turbulence is investigated. Results of direct numerical simulations (DNS) of homogeneous sheared turbulence with uniform stable (supercritical) stratification are used in the analysis. Two cases are considered: HB-NISF, in which there is no initial fluctuating G, and HB-ISF, in which strong initial fluctuating G is present. The triadic interaction at the primary level involves the direct coupling of paired mechanisms. Interaction of ω and S is characterized by vortex stretching and locally-induced rotation of the S axes which are both influenced by mean ω and S. At early time, S axes rotation is enhanced in HB-ISF due to baroclinic torque generation of ω by initial G. In HB-NISF, S axes rotation is impeded. In time, the behavior of HB-ISF becomes similar to HB-NISF and shows limited vortex stretching. Interaction of ω and G involves an inherent negative feedback between baroclinic torque and reorientation of G by ω. The initial G in HB-ISF causes baroclinic torque to act as a source of ω early in time. Later, the inherent negative feedback in HB-NISF is established and baroclinic torque becomes a sink. Interaction of S and G is characterized by a positive feedback between differential acceleration and scalar gradient amplification by compressive straining. In HB-ISF, this interaction is strong due to the high amplitude of initial G and results in persistent G^2. In general, the behavior of ω, S, and G in HB-ISF tends towards that of HB-NISF as the flow settles into a similar state of decay.

INTRODUCTION

An important aspect of turbulence is vortex stretching, that is, the interaction of vorticity ω and rate-of-strain S. Characteristics of ω and S are therefore of considerable interest. Direct numerical simulations (DNS) of homogeneous turbulence have revealed various properties of ω and S and the presence of distinct small-scale structure (see review in Nomura and Post (1998)). The associated dynamics of ω and S are described in the principal strain basis which effectively distinguishes vortex stretching and rotation of the principal axes of S (Nomura and Post, 1998). In homogeneous shear, these mechanisms are influenced by the imposed mean ω and S and, consequently, result in preferential spatial orientation of ω and the principal axes (Nomura and Diamessis, 1999).

In the presence of shear and stratification (mean density gradient), directional features in ω and S will influence the behavior of the fluctuating density gradient, $G \equiv \nabla\rho$. When buoyancy effects are signficant, the dynamics of G will feedback on ω and S. Previous DNS of stratified homogeneous shear flow (Gerz, 1991) show a predominance of horizontal ω which manifests itself as a *collapse* of vortex structures in the flow. The dynamics associated with the collapse and, more generally, the fully coupled interaction of ω, S, and G, have recently been investigated (Diamessis and Nomura, 1999). Key physical mechanisms and their interactions are identified. In these simulations, scalar fluctuations are not initially present and the dynamics at early time involve the generation of G by ω and S, both of which possess preferential orientation due to mean shear effects. The resulting structure in ω, S, and G is strongly directional due to the combined effects of shear and buoyancy. In order to extend our understanding of the coupled system, we investigate the influence of an initial, nearly isotropic G field on ω and S and the associated feedback. Such conditions may arise, for example, in the ocean where turbulence interacts with scalar fluctuations resulting from a density overturn of large spatial extent. We note that the effect of initial scalar fluctuations in stratified turbulent flows has previously been examined (Hunt et al., 1988; Gerz and Schumann, 1988; Holt et al., 1992), however, only large-scale quantities are considered. In this work, we are interested in small-scale, i.e., gradient quantities. Results from DNS of

stratified shear flow with and without initial scalar fluctuations are presented. We first review the general dynamics associated with ω, S, and G.

DYNAMIC INTERACTION

In the presence of stratification and buoyancy, the fluid density ρ is an active scalar. The behavior of ω and S is then influenced by the fluctuating gradient of ρ, $G \equiv \nabla\rho'$, and ω, S, and G represent a fully coupled triadic system with complex feedback mechanisms. The associated evolution equations (Boussinesq approximation) are,

$$\frac{D\omega_i}{Dt} = \underbrace{S_{ik}\omega_k}_{\text{vortex stretching}} + \nu\frac{\partial^2\omega_i}{\partial x_k \partial x_k} \underbrace{- \frac{g}{\rho_0}\varepsilon_{ij3}G_j}_{\text{baroclinic torque}} \quad (1)$$

$$\frac{DS_{ij}}{Dt} = -S_{ik}S_{kj} - \tfrac{1}{4}\underbrace{(\omega_i\omega_j - \delta_{ij}\omega_k\omega_k)}_{\text{strain gen./rot.}} - \frac{1}{\rho}\frac{\partial^2 p}{\partial x_i \partial x_j}$$

$$+ \nu\frac{\partial^2 S_{ij}}{\partial x_k \partial x_k} \underbrace{- \frac{g}{2\rho_0}(G_j\delta_{i3} + G_i\delta_{j3})}_{\text{differential acceleration}} \quad (2)$$

$$\frac{DG_i}{Dt} = \underbrace{-S_{ik}G_k}_{\text{straining}} + \underbrace{\tfrac{1}{2}\varepsilon_{ijk}\omega_j G_k}_{\text{reorientation}} + D\frac{\partial^2 G_i}{\partial x_k \partial x_k} \quad (3)$$

Key terms associated with the fully coupled interaction are underbraced. Interaction between ω and S include vortex stretching and strain generation and axes rotation (1)-(2). Influence of ω and S on G is through amplification/attenuation by S and reorientation by ω (3). In the presence of buoyancy, there is direct feedback of G on ω through baroclinic torque (1) and on S through differential acceleration (2). Thus, at the primary level, the triadic interaction includes the coupling of the following mechanisms: vortex stretching and strain axes rotation and generation (ω and S), gradient reorientation and baroclinic torque (ω and G), and gradient amplification and differential acceleration (S and G). At the secondary level, various repercussions of these coupled mechanisms will occur. The results presented will demonstrate the predominant interactions.

DIRECT NUMERICAL SIMULATIONS

Homogeneous sheared turbulence with uniform stable stratification is considered in this study. Figure 1 shows profiles of the mean velocity $U(x_3)$ and density $\overline{\rho}(x_3)$. The mean gradients are denoted by $dU/dx_3 = S$ and $d\overline{\rho}/dx_3 = \overline{G_3}$. Relevant nondimensional parameters include the turbulent Reynolds number based on the Taylor microscale, $Re_\lambda = u\lambda/\nu$, and the shear number, $Sh = (u^2/\varepsilon)/(1/S)$. Here, u is the r.m.s. velocity, ε is the energy dissipation rate, and ν is the kinematic viscosity. The relative significance of stratification to mean shear effects is characterized by the Richardson number, $Ri = N^2/S^2 = (-g\,\overline{G_3}/\rho_0)/S^2$, where N is the Brunt-Vaisala frequency, g is the acceleration of gravity, and ρ_0 is a reference density. Initial scalar fluctuations are specified in terms of the *energy partition ratio* (Hunt et al., 1988), $\eta \equiv \langle\rho^2\rangle N^2 / \langle u_3^2\rangle \overline{G_3}^2$, which is the ratio of potential energy to vertical kinetic energy. Here, $\langle\rho^2\rangle$ and $\langle u_3^2\rangle$ are the mean square values of fluctuating density and vertical component velocity, respectively.

The governing equations describing the flow are the time-dependent continuity and Navier-Stokes equations with the Boussinesq approximation. The computational domain contains 128^3 grid points. Periodic boundary conditions are employed in the x_1 (streamwise) and x_2 (spanwise) directions and shear-periodic conditions in the x_3 (mean gradient) direction (Gerz et al., 1989). The simulations are initialized with a fully developed isotropic turbulent velocity field. The initial scalar field is obtained by allowing isotropic scalar fluctuations to develop with the isotropic velocity in the presence of $\overline{G_3}$ but without gravity and external shear forces. The initial G field is thus slightly anisotropic. The numerical solution employs a pseudospectral method (Gerz et al., 1989).

In the results presented here, initial parameter values are $Re_{\lambda_o} = 20$ and $Sh_o = 3.2$. Simulations are performed for flow with no buoyancy ($Ri = 0$, NB) and with strong buoyancy ($Ri = 1$, HB). The HB flow is thus supercritically stratified. In cases denoted by NISF, there are no initial scalar fluctuations ($\eta_0 = 0$). In cases denoted by ISF, $\eta_0 = 8$, thus initial scalar fluctuations are significant. This η_0 value is comparable to that used previously (Holt et al., 1992) which produced marked deviations in the early time flow behavior. The general large-scale flow behavior is as follows. In the NB flow, beyond a short period of decay due to initial isotropic conditions, the turbulent kinetic energy (TKE) increases in time eventually exhibiting an asymptotic increase. For $Ri = 1$ with $\eta_0 = 0$ (HB-NISF), TKE rapidly decays. In the flow with $Ri = 1$ and $\eta_0 = 8$ (HB-ISF), TKE decays for a very short time as its vertical component is converted into potential energy (PE). The TKE then begins to increase to the expense of the large PE of the initial scalar fluctuations. At time $St \approx 2$, TKE and ε reach their peak values. Beyond this time, TKE and ε monotonically decay and eventually, exhibit similar rate of decay as that of HB-NISF.

RESULTS

The time evolution of the r.m.s. components of G for each of the simulated flows is shown in Fig. 2a,c. Note that in the case of ISF, $G_o'/\overline{G_3} = 4.3$, indicating the significance of the initial fluctuating G field. We see that in the case of NB-ISF (Fig. 2a), the components of G decay in time until they converge to those of NB-NISF which eventually increase. In HB-ISF (Fig. 2c), initially there is a rapid decay. Later, the rate of decay is reduced considerably and stabilizes to that of the HB-NISF case. Note, however, that the higher $|G|$ persists in HB-ISF. The evolution of the r.m.s. components of fluctuating ω is shown in Fig. 2b,d (note that hereafter, ω will denote the fluctuating component while S refers to the total S). In the

NB flow (Fig. 2b), initially, ω_1 and ω_3 prevail due to amplification by mean strain while later, ω_2 increases due to amplification by fluctuating strain. In the HB-NISF flow (Fig. 2d), buoyancy effects are significant. At very early time ($St < 1$), the behavior is similar to NB. Beyond this initial time, ω_3 exhibits an enhanced rate of decay leaving horizontal components ω_1 and ω_2 to dominate. All three components continue to decay in time. In the HB-ISF flow (also Fig. 2d), the presence of strong initial G generates intense ω_1 and ω_2 which are then subjected to the mean shear. As a result, ω_1 rapidly increases due to amplification by mean strain. Component ω_3 initially decreases and then increases due to shear effects and transfer from ω_1. Eventually however, buoyancy effects take over and result in a prevalence of horizontal ω which decays at a rate similar to that of HB-NISF. The behavior of HB-NISF is described elsewhere (Diamessis and Nomura, 1999). Here, we focus particularly on the physics during the early transient in which the behavior of HB-ISF distinctively differs.

In order to assist the analysis of the complex interaction of ω, S, and G, conditional sampling based on the invariants of the velocity gradient tensor is employed (Diamessis and Nomura, 1999). Recall for an incompressible flow, the first invariant is $I = 0$, and the second and third invariants are $II = (\omega^2/2 - S^2)/2$ and $III = -\alpha\beta\gamma - (\alpha\omega_\alpha^2 + \beta\omega_\beta^2 + \gamma\omega_\gamma^2)/4$, respectively, where α, β, γ, are the eigenvalues of S. Thus, II indicates the relative significance of ω and S. As in our previous work (Diamessis and Nomura, 1999), we will consider high amplitude conditional samples which are referred to by the particular quadrant of the $II - III$ plane. Thus, sample QII consists of high-amplitude rotation-dominated events ($II > 0$, $III < 0$) while sample QIV consists of high-amplitude strain-dominated events ($II < 0$, $III > 0$). In addition, we consider a sample Q0 which consists of high-amplitude events (high ω^2) with comparable rotation and strain ($II \approx 0$). These conditional samples effectively resolve various mechanisms by considering the relative significance of rotation versus strain. Previous work showed that the combined behavior of the high amplitude events effectively describe the behavior of the total flow (Diamessis and Nomura, 1999).

As discussed earlier, the development of directional features plays an important role in the coupled dynamics of these flows. We therefore examine the spatial orientation of ω, S (eigenvectors), and G. The orientation of a vector $\vec{V}$ in cartesian coordinate space can be defined by the angle pair $(\theta_{pitch}, \theta_{yaw})$ where θ_{pitch} is the angle of $\vec{V}$ from its projection on the $x_1 - x_2$ (horizontal) plane and θ_{yaw} is the angle of the projection on the $x_1 - x_2$ plane from the positive x_2-axis (Fig. 3). The joint probability distribution (jpd), $(\sin(\theta_{pitch}), \theta_{yaw})$, effectively indicates the most probable orientation for a given sample (Nomura and Diamessis, 1999). Figure 4a-c shows the orientation of ω at $St = 2$. In all three flows, $|\theta_{pitch}| < 45°$ and $|\theta_{yaw}| > 90°$ prevail. At this time, HB-ISF (Fig. 4c) exhibits the lowest θ_{pitch} values which indicates the prevalence of horizontal ω consistent with Fig. 2d. Note that the shape of the distributions in HB-ISF resembles that in NB (Fig. 4a).

In order to understand the underlying behavior, we first consider the primary interaction between ω and S. This is described in detail elsewhere (Nomura and Diamessis, 1999) and here we summarize the main points. The associated dynamics are described by considering Eqs. (1)-(2) in the principal strain basis. Here, we define the principal eigenvalues by $\alpha \geq \beta \geq \gamma$ and denote the corresponding eigenvectors, e_α, e_β, e_γ. In addition to interaction through vortex stretching, ω and S interact through locally- and nonlocally-induced rotation of the principal axes of S and through generation of strain. The induced rotations are associated with misaligned ω with respect to the S axes and the sense of rotation is such to orient ω towards either e_β or e_γ (Nomura and Post, 1998). In the early development of the shear flow, amplification of fluctuating ω in the direction of the extensional strain of the mean shear, $\bar{e}_\alpha$, prevails. The presence of $\bar{\omega} = S$ establishes a predominant misalignment of ω (Fig. 5a) which results in locally-induced rotation of the S axes. If the eigenvectors of S initially coincide with those of the mean shear, i.e., $\bar{e}_\alpha$, $\bar{e}_\beta$, and $\bar{e}_\gamma$, the induced rotation will reorient e_α and e_β in the plane comprised of $\bar{e}_\alpha$ and $\bar{e}_\beta$. This plane, referred to as $S^+ -$ plane, corresponds to a reverse "S"-shaped curve in the $(\sin(\theta_{pitch}), \theta_{yaw})$ plot (Fig. 5b). The sense of rotation is such that e_β is directed towards ω. Further amplification of ω will occur along the reoriented principal axes and thus we expect ω to orient accordingly in the $S^+ -$ plane. The distributions in Fig. 4a,c are generally consistent with the described dynamics, in particular, in the prevalence of $|\theta_{pitch}| < 45°$ and $|\theta_{yaw}| > 90°$. The presence of ω in other directions (isotropic initial conditions) will cause the rotation of the S axes to vary which results in the observed distributions. Note that misaligned ω in the $\bar{e}_\beta$-$\bar{e}_\gamma$ plane induces rotation of e_γ and e_β about the axis of e_α. The associated $S^- -$ plane ($\bar{e}_\beta$-$\bar{e}_\gamma$) corresponds to a *forward* S-shaped curve in the two angle plot. The jpds for the Q0 conditional sample are shown in Fig. 4d-f. The $S^+ -$ plane curve attribute is more evident. An even greater distinction is exhibited by the QIV sample (not shown). This is due to enhancement of locally-induced axes rotation in high S^2 regions (Nomura and Diamessis, 1999). Note the similarity of the behavior of HB-ISF to that of NB. In fact, interaction of ω and S is enhanced in the HB-ISF flow. Probability distributions of the eigenvalues of S (not shown) indicate higher magnitudes. In time, as in HB-NISF, the distributions become more symmetric about zero and $\langle\beta\rangle$ is reduced. The third invariant III tends towards zero indicating reduced vortex stretching.

We now consider the primary interaction of ω and G. This is most clearly demonstrated by rotation-dominated QII events. In HB-NISF, G is initially generated by sheared turbulence. In QII regions, this is through reorientation of $\overline{G_3}$ by prevailing ω. During early development, baroclinic torque will generate ω of *opposite sign* to that which gave rise to G and thus effectively acts as a sink for ω_1 and ω_2. In case HB-ISF, baroclinic torque is generated by an already established, nearly isotropic G and this represents a source of horizontal ω. This is consistent with the results in Fig. 4c which indicates enhanced horizontal ω at early time. The generated ω is then subjected to interaction with S and mean shear and $S^+ -$ plane dynamics occur. Later in time, the inherent negative feedback mechanism in HB-NISF is established and baroclinic torque then acts as a sink of ω promoting decay (Fig. 2d).

Figure 6 shows the orientation of e_β and e_γ for each of the

flows. In NB, the distributions for e_β (Fig. 6a) generally follow the $S^+ -$ plane curve while e_γ (Fig. 6d) generally follows the $S^- -$ plane curve. In HB-NISF (Fig. 6b,e), there is reduced variation in the spatial orientation of the eigenvectors. This is a result of baroclinic torque which generates ω_2 and effectively impedes locally-induced rotation of the S axes by reducing the misalignment of ω. Although ω_1 is also generated, ω_2 is stronger due to the directional preference established in the generated G. In HB-ISF (Fig. 6c,f), rotation of the S axes is enhanced. As discussed, the initial G generates strong ω_1 and ω_2. In particular, ω_1 is subjected to straining along $\bar{e}_\alpha$ and this reinforces the misalignment of ω. In addition, there is increased probability of ω to orient in the $S^- -$ plane and thus we see greater variation in e_γ (Fig. 6f). Note that the probable orientation of e_γ for HB-ISF tends towards higher θ_{pitch} values.

The primary interaction between S and G is now considered. As indicated in Eq. (2), differential acceleration can enhance compressive straining when high density fluid occurs above that of low density, i.e., positive vertical gradient $+G_3$. Figure 7a,d shows the orientation of G for the total flow of HB-NISF and HB-ISF. As indicated, there is a prevalence of $+G_3$ ($\theta_{pitch} \rightarrow +90°$, lower right quadrant) in both HB flows. In NB-NISF (not shown), this is attributed to initial generation of G through reorientation by ω as indicated by QII events (Diamessis and Nomura, 1999). In strain-dominated regions (QIV), initial generation of G is through amplification along e_γ which results in high probability in the upper left quadrant of the jpd ($-G_3$). These trends are generally exhibited by the QII and QIV samples for HB-NISF (Fig. 7b,c). The persistence of $+G_3$ (high probability in lower right quadrant) in QIV in the HB flows is due to differential acceleration. Since compressive straining is strong in QIV regions, $|G|$ is significant. The presence of $+G_3$ will enhance $-S_{33}$ through differential acceleration (2). This promotes vertical compressive straining (Fig. 6f) which will amplify $+G_3$ and thus establish a positive feedback mechanism. In HB-ISF (Fig. 7e), the persistence of $+G_3$ is stronger due to the high-amplitude $+G_3$ initially present which establishes a stronger feedback earlier in time. This is supported by examining the jpd of S_{33} and G_3 (Fig. 8b) which shows high magnitude $+G_3$ associated with high magnitude $-S_{33}$. Note that this correlation is not present in the NB-ISF flow (Fig. 8a). In addition, in the QII sample of HB-ISF (Fig. 7f), orientation of G exhibits significant variation while generally following e_γ (Fig. 6f). Since ω did not originally generate G, it does not tend to control its orientation. The positive feedback of G and S acts to sustain G^2 and explains the observed behavior in HB-ISF at later times (Fig. 2c).

CONCLUSIONS

We have investigated the fully coupled triadic interaction of ω, S, and G in stably stratified homogeneous sheared turbulence. At the primary level, the interaction involves the direct coupling of the following mechanisms: vortex stretching and strain generation and axes rotation (ω and S), gradient reorientation and baroclinic torque (ω and G), and gradient amplification and differential acceleration (S and G). In order to develop a more complete understanding of the coupled system, the behavior of two distinct cases are compared: HB-NISF, in which fluctuating G is not initially present but produced by the prevailing ω and S, and HB-ISF, in which strong initial fluctuating G is present. The results presented demonstrate the predominant interactions.

Interaction of ω and S is characterized by vortex stretching and locally-induced rotation of the S axes which are both influenced by the presence of mean ω and S. At early time, S axes rotation is enhanced in HB-ISF due to baroclinic torque generation of ω. In HB-NISF, S axes rotation is impeded due to the inherent directional preference in baroclinic torque in this case. In time, the behavior of HB-ISF becomes similar to HB-NISF as these preferences become established. The third invariant III tends towards zero indicating reduced vortex stretching. Interaction of ω and G involves an inherent negative feedback between baroclinic torque and reorientation of G by ω. This is quickly established in HB-NISF and causes baroclinic torque to act as a sink. The presence of an initial G field in HB-ISF allows baroclinic torque to provide a source of ω early in time. Later, the inherent negative feedback is established and baroclinic torque becomes a sink. Finally, interaction of S and G is characterized by a positive feedback between differential acceleration and scalar gradient amplification by compressive straining. In HB-ISF, this interaction is strong due to the high amplitude of initial G and results in persistent G^2. Overall, the influence of initial scalar fluctuations is active only for a transient period after which the flow settles into a state of decay, similar to that of HB-NISF.

REFERENCES

Diamessis, P. J. and Nomura, K. K. (1999). Interaction of vorticity, rate of strain, and scalar gradient in stratified homogeneous sheared turbulence. *In preparation.*

Gerz, T. (1991). Evolution of coherent vortex structures in sheared and stratified homogeneously turbulent flows. Munich, Germany. Eighth Symposium on Turbulent Shear Flows.

Gerz, T. and Schumann, U. (1988). In 'Finite approximations in fluid mechanics, Part 2'. pages 142–155, Vieweg. (Ed. E. Hirschel).

Gerz, T., Schumann, U., and Elghobashi, S. (1989). Direct simulation of stably stratified homogeneous turbulent shear flows. *J. Fluid Mech.*, 200:563–594.

Holt, S. E., Koseff, J. R., and Ferziger, J. H. (1992). A numerical study of the evolution and structure of homogeneous stably stratified sheared turbulence. *J. Fluid Mech.*, 237:499–539.

Hunt, J. C. R., Stretch, D. D., and Britter, R. E. (1988). In 'Stably stratified flow and dense gas dispersion'. pages 285–321, Clarendon Press. (Ed. J. S. Puttock).

Nomura, K. K. and Diamessis, P. J. (1999). The interaction of vorticity and rate of strain in homogeneous sheared turbulence. *Submitted to Phys. Fluids.*

Nomura, K. K. and Post, G. K. (1998). The structure and dynamics of vorticity and rate of strain in incompressible homogeneous turbulence. *J. Fluid Mech.*, 377:65–97.

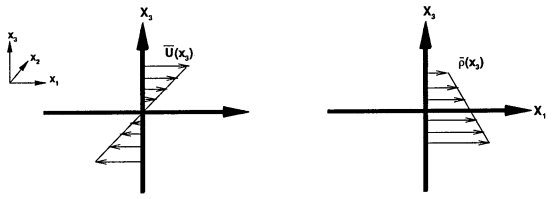

Figure 1. Sketch of mean velocity and density profiles and coordinate system.

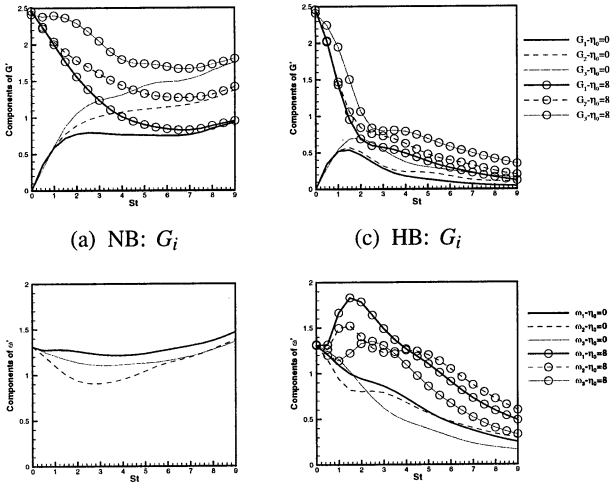

(a) NB: G_i (c) HB: G_i

(b) NB: ω_i (d) HB: ω_i

Figure 2. Time evolution of fluctuating components of G and ω for NB and HB flows (plain lines: NISF, circles (○): ISF).

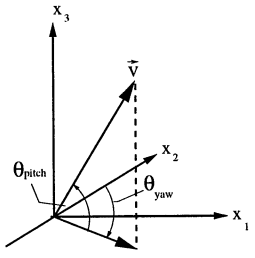

Figure 3. Definition of the angles of orientation $(\theta_{pitch}, \theta_{yaw})$ of a vector in 3-D cartesian coordinates.

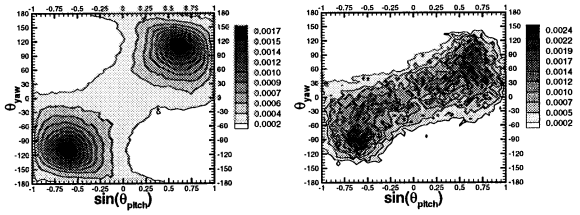

(a) NB (d) NB: Q0

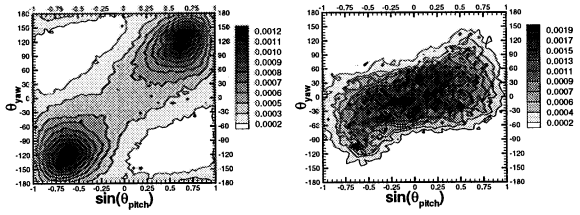

(b) HB-NISF (e) HB-NISF: Q0

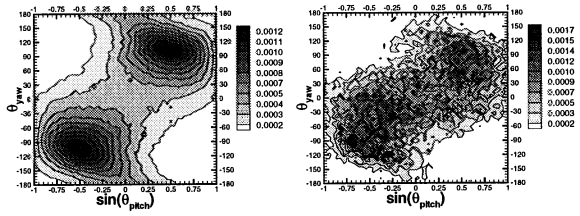

(c) HB-ISF (f) HB-ISF: Q0

Figure 4. Joint probability distributions indicating the angles of orientation of fluctuating ω for total flow (a-c) and conditional samples (d-f).

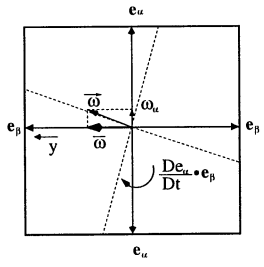

(a)

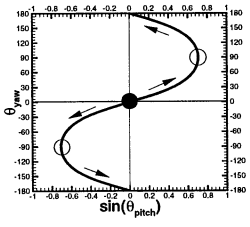

(b)

Figure 5. Description of $S-$plane: (a) diagram of S^+- plane indicating locally-induced rotation of the principal axes, (b) S^+-plane curve on $\sin(\theta_{pitch})$ vs θ_{yaw} plot (open circles (○) correspond to orientation of $\bar{e}_\alpha$, full circle (•) that of $\bar{e}_\beta$).

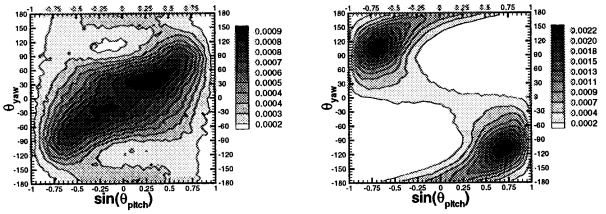

(a) e_β: NB (d) e_γ: NB

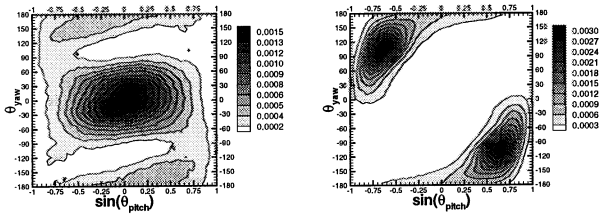

(b) e_β: HB-NISF (e) e_γ: HB-NISF

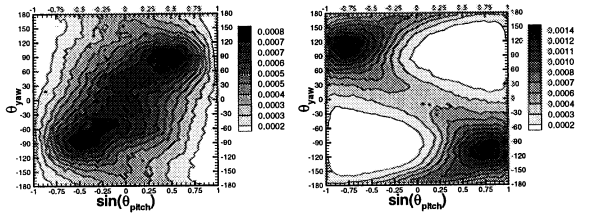

(c) e_β: HB-ISF (f) e_γ: HB-ISF

Figure 6. Joint probability distributions indicating the angles of orientation of e_β and e_γ for total flow at $St = 2$.

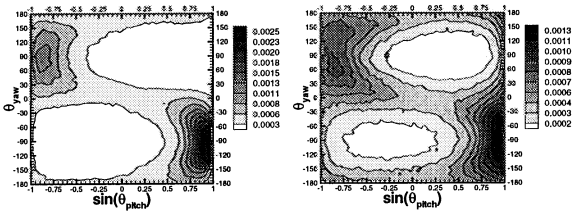

(a) HB-NISF: Total flow (d) HB-ISF: Total Flow

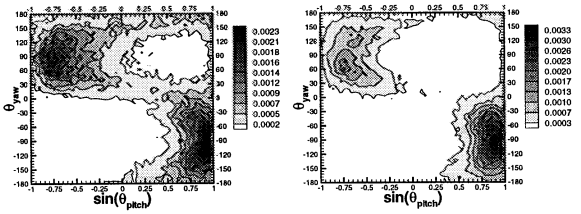

(b) HB-NISF: QIV (e) HB-ISF: QIV

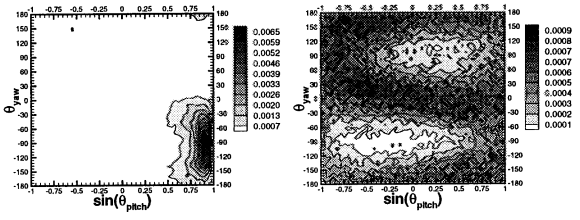

(c) HB-NISF: QII (f) HB-ISF: QII

Figure 7. Joint probability distributions indicating the angles of orientation of fluctuating G at $St = 2$.

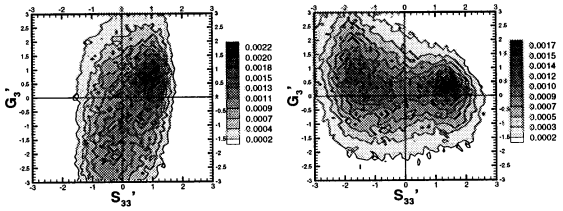

(a) NB-ISF (b) HB-ISF

Figure 8. Joint probability distribution of the values of S_{33} and G_3 for $\eta_0 = 8$ at $St = 2$ (QIV sample).